



1 **Intense $p\text{CO}_2$ and $[\text{O}_2]$ Oscillations in a Mussel-Seagrass Habitat:**
2 **Implications for Calcification.**

3

4 **Vincent Saderne^{1,2}, Peer Fietzek^{1,3}, Jens Daniel. Müller⁴, Arne Körtzinger^{1,5} and**
5 **Claas Hiebenthal¹**

6 [1]{GEOMAR Helmholtz Centre for Ocean Research Kiel, Kiel, Germany}

7 [2]{KAUST King Abdullah University of Science and Technology, Thuwal, Kingdom of Saudi
8 Arabia}

9 [3]{Kongsberg Maritime Contros GmbH, Kiel, Germany}

10 [4]{Leibniz Institute for Baltic Sea Research, Warnemünde, Germany}

11 [5]{Christian Albrecht University, Kiel, Germany}

12 Correspondence to: V. Saderne (vincent.saderne@KAUST.edu.sa)

13

14 **Abstract**

15 Numerous studies have been conducted on the effect of ocean acidification on calcifiers inhabiting
16 nearshore benthic habitats, such as the blue mussel *Mytilus edulis*. The majority of these
17 experiments was performed under stable CO_2 partial pressure ($p\text{CO}_2$), carbonate chemistry and
18 oxygen (O_2) levels, reflecting present or expected future open ocean conditions. Consequently,
19 levels and variations occurring in coastal habitats, due to biotic and abiotic processes, were mostly
20 neglected, even though these variations largely override global long-term trends. To highlight this
21 hiatus and guide future research, state-of-the-art technologies were deployed to obtain high-
22 resolution time series of $p\text{CO}_2$ and $[\text{O}_2]$ on a mussel patch within a *Zostera marina* seagrass bed,
23 in Kiel Bay (western Baltic Sea) in August and September 2013. Combining the in situ data with
24 results of discrete sample measurements, a full seawater carbonate chemistry was derived using
25 statistical models. An average $p\text{CO}_2$ more than 50% ($\sim 640 \mu\text{atm}$) higher than current atmospheric
26 levels was found right above the mussel patch. Diel amplitudes of $p\text{CO}_2$ were large: 765 ± 310
27 (mean \pm SD). Corrosive conditions for calcium carbonates (Ω_{arag} and $\Omega_{\text{calc}} < 1$) centered on sunrise



28 were found, but the investigated habitat never experienced hypoxia throughout the study period. It
29 is estimated that mussels experience conditions limiting calcification for 12 - 15 h per day, based
30 on a regional calcium carbonate concentration physiological threshold. Our findings call for more
31 extensive experiments on the impact of fluctuating corrosive conditions on mussels. We also stress
32 the complexity of the interpretation of carbonate chemistry time series data in such dynamic coastal
33 environments.

34

35

36 **1 Introduction**

37 Since preindustrial times, the atmospheric CO₂ mixing ratio rose from approximately 280 ppmv
38 to actual ~400 ppm (Mauna Loa, annual mean 2016, NOAA-ESRL). Future climate scenarios
39 predict a strong further increase of up to 1000 ppm by the year 2100 (IPCC, 2013). The dissolution
40 of anthropogenic CO₂ in seawater causes an increase in the seawater CO₂ partial pressure (*p*CO₂)
41 and a concurrent decrease of the seawater pH, a global phenomenon also referred to as ocean
42 acidification (OA) (Bates et al., 2014 and Doney et al., 2009).

43 OA reduces the supersaturation of seawater with respect to calcite and aragonite, which may cause
44 seawater to become corrosive for these calcium carbonates, that compose the shells and skeletons
45 of marine species (see Harvey et al., 2013 and Andersson et al., 2011 for review and meta-
46 analysis). In their review, Wahl et al. (2015) counted a total of 350 studies on the response of
47 benthic marine fauna and flora to ocean acidification, either in the field or in mesocosms. The
48 majority of these studies considered open ocean pH and *p*CO₂ as reference for the scenarios
49 employed to study the impact of OA. Indeed, the carbonate system (pH, *p*CO₂, dissolved inorganic
50 carbon (DIC) and total alkalinity (TA)) in surface oceans is understood relatively well, and many
51 models exist predicting the future rise of *p*CO₂ and decrease of pH (e.g. Orr et al., 2005). However,
52 very recent articles highlight the inapplicability of these predictions for the nearshore environment
53 (Duarte et al., 2013; Wahl et al., 2015; Müller et al., 2016) and the serious lack of relevant datasets
54 for the different major types of benthic habitats worldwide (Wahl et al., 2015). In addition to OA,
55 ocean warming and eutrophication of coastal waters around the world cause a spreading and
56 shoaling of hypoxia ([O₂] < 60 μmol kg⁻¹) in the ocean's interior (Diaz and Rosenberg, 2008;
57 Keeling et al., 2010).



58 In nearshore areas, metabolic processes by flora and fauna (photosynthesis, respiration and
59 calcification) and redox reactions in the sediment (e.g. sulfate reduction/sulfide oxidation,
60 denitrification/nitrification) strongly affect the carbonate chemistry of the water column,
61 temporarily generating strong disequilibria for CO₂ and O₂ between the sea and the atmosphere.
62 Cycles of super- and undersaturation for these two metabolic gases have been observed in all kinds
63 of benthic habitats at daily and seasonal scale, but also in relation to physical forcing such as tides,
64 wind or precipitation (Hofmann et al., 2011; Saderne et al., 2013; see Wahl et al., 2015 for review).

65 As an example, in the western Baltic Sea (Eckernförde Bay) Saderne et al. (2013) found daily
66 variations of *p*CO₂ of 200 - 400 μatm between July and September in a macrophyte meadow
67 dominated by the brown algae *Fucus serratus*, with maximum *p*CO₂ levels reaching up to
68 approximately 2200 μatm during upwelling conditions. As a consequence, seawater saturation
69 states for calcite and aragonite (Ω_{calc} and Ω_{arag}) repeatedly fell below the dissolution threshold (Ω
70 < 1, i.e. seawater turning undersaturated and hence corrosive to these biominerals) during the
71 upwelling event, which was monitored over several days.

72 Here, we present a case study of a mixed seagrass/mussel bed, illustrating the carbonate chemistry
73 conditions typically experienced by calcifiers in their natural habitat. We measured *p*CO₂ and
74 dissolved oxygen ([O₂]) directly above a mussel patch of less than 2 m² extension, surrounded by
75 seagrass, in a mosaic seagrass-mussel habitat as it is characteristic for western Baltic Sea nearshore
76 benthic habitats. We used a combination of autonomous in situ sensors for *p*CO₂, [O₂], salinity
77 and temperature, complemented by discrete sampling for DIC, TA, phosphate, and silicate, for a
78 period of more than 7 weeks in summer 2013. Using statistical modeling, we derived time series
79 for the entire study period for carbonate chemistry parameters including Ω_{calc} and Ω_{arag} . Based on
80 literature knowledge regarding effects of carbonate ion concentration ([CO₃²⁻]) as well as Ω_{calc} and
81 Ω_{arag} effects on mussel biomineralization, we identified time windows of potentially favorable and
82 unfavorable conditions for mussel calcification.

83

84 **2. Materials and Methods**

85 **2.1 Description of Kiel Bay and the experimental site**



86 Kiel Bay is a narrow and shallow bay in the western Baltic Sea that consists of two basins. The
87 inner Kiel Bay (see Fig. 1A) in the south is up to approximately 2 km wide and (except for a few
88 deeper dips) up to 14 m deep, while the outer Kiel Bay is up to approximately 5 km wide and
89 approximately 20 m deep and opens in the north to the larger Kiel Bight (Kögler and Ulrich, 1985;
90 Schwarzer and Themann, 2003). Surface and bottom water bodies of the larger Kiel Bight swash
91 in and out Kiel Bay (mainly driven by varying wind directions and intensities). Freshwater influx
92 from the small river “Schwentine” (east side of Kiel Bay, opposite to GEOMAR on Fig. 1A) also
93 shapes the hydrology of the inner Kiel Bay. The strict separation of deep and shallow water bodies
94 by stratification in the larger Kiel Bight and its bays that typically occurs during summer months
95 is occasionally broken-up by wind-driven upwelling. The shallow coastal communities are then
96 put in contact with high CO₂ and sometimes hypoxic sub-surface waters (Feely et al., 2008;
97 Melzner et al., 2013).

98 In Kiel Bay, as in several other enclosed bays of the western Baltic Sea, the blue mussel *Mytilus*
99 *edulis* and the seagrass *Zostera marina* co-occur in patches forming mosaic habitats (Reusch and
100 Chapman, 1995; Vinther et al., 2008; Vinther and Holmer 2008; Vinther et al. 2012). A sensor
101 package measuring pCO₂, [O₂], salinity and temperature was deployed at 2 m depth in a mixed
102 habitat formed by *Z. marina* and *M. edulis* in Kiel Bay, western Baltic Sea (54.3467 °N,
103 10.1539 °E; see Fig.1A). The package was directly placed on a mussel patch within the seagrass
104 bed. The deployment was conducted for 50 days from the 08.08.2013 to 27.09.2013 with short
105 power interruptions from 10.08., 17:10 to 11.08., 8:00 and from 12.08., 5:00 to 14.08., 16:00.

106 **2.2 In situ sensor suite**

107 Temperature, salinity and [O₂] were measured simultaneously every 10 min with a SBE 37–SI
108 MicroCAT (temperature and salinity, Sea-Bird Electronics Inc., USA) and an oxygen optode
109 Aanderaa 3835 (Aanderaa Data Instruments AS, Norway) enclosed in a flow cell. The circulation
110 of water between the SBE 37–SI and the optode was achieved by means of an SBE 5M pump
111 (Sea-Bird Electronics Inc., USA) that ran for 30 seconds every 10 min. The coordination of
112 pumping and recording by the SBE 37 and the optode was carried out by a custom-made data
113 logger (Todd Martz Laboratory, Scripps Institution of Oceanography, San Diego, USA). To
114 prevent fouling on sensors, the SBE 37–SI was equipped with tributyltin tablets and copper tubing
115 linked the SBE 37–SI and the flow cell to the pump.



116 A HydroC[®] CO₂ II sensor (KM Contros GmbH, Kiel, Germany) was used to autonomously
117 measure in situ CO₂ partial pressure (*p*CO₂). The sensor determines *p*CO₂ optically by means of
118 an nondispersive infrared (NDIR) absorption measurement within a membrane-equilibrated
119 headspace (Fietzek et al., 2014). The sensor was calibrated at a water temperature of 17.5 °C at 6
120 different *p*CO₂ levels across a measurements range of 200 - 2200 μatm by the manufacturer before
121 (July) and after (November) the measurements. The corresponding calibration polynomials had a
122 quality of $R^2 = 0.999998$ and 0.99998 with root mean square errors of 1.15 and 3.98 ppm.
123 Calibrations and data processing were carried out according to Fietzek et al. (2014) with the
124 exception that, here, the interpolation between the pre- and the post-deployment calibration
125 polynomial was carried out according to the sensor's absolute run-time between the two
126 calibrations.

127 During the field deployment, the sensor was powered from the nearby pier. Data were stored
128 internally on its data logger. The sensor was configured to carry out a 2 min zeroing every 6 h. A
129 flushing interval duration of 55 min was used to analyze the data during recovery from zero to
130 ambient values. During the subsequent measurement interval, a 10 s mean of the 1 Hz raw data
131 was stored every minute.

132 The HydroC[®] was equipped with a flow-head allowing for passive diffusion of seawater to the
133 sensor's membrane through a circumferential orifice along the cylindrical sensor housing. In order
134 to improve the data quality under the given configuration and deployment conditions,
135 determination and correction of the sensor's response time (RT) were given special attention (see
136 Appendix A for further information). The sensor's in situ RT was determined to be 546 ± 208 s
137 (mean \pm SD) and the final *p*CO₂ series was response time corrected assuming a constant RT of
138 546 s.

139 We conclude a general uncertainty for the final *p*CO₂ series in this study of 2.5% of reading as the
140 standard deviation of the *p*CO₂ measurements. This value is comprised of the accuracy of drift
141 corrected HydroC[®] *p*CO₂ data of approximately 1% of reading as found within Fietzek et al. (2014)
142 and the uncertainty estimate of 1.5% of reading related to the actual RT influences (see Appendix
143 A).

144 **2.3 Discrete sampling**



145 Over the course of the deployment, a total of 31 seawater samples for DIC and TA were taken at
146 the sensor suite through snorkeling. Sampling was conducted twice a week in the hours following
147 sunrise and solar noon. On a third day, duplicate sampling was conducted in the hour following
148 solar noon. Corresponding sampling results were averaged to improve the quality of the
149 measurements. Salinity of the water samples was measured in a laboratory at GEOMAR using a
150 conductometer (SG 7/8, Mettler Toledo, Switzerland). Subsequently, the samples were poisoned
151 with mercury chloride following the recommendations by Dickson et al. (2007). DIC (precision \pm
152 $3 \mu\text{mol kg}^{-1}$) was measured by coulometry using a SOMMA instrument (University of Rhode
153 Island, USA) and TA (precision $\pm 6 \mu\text{mol kg}^{-1}$) was determined with a VINDTA titrator (Marianda
154 GmbH, Germany) following Dickson et al. (2007).

155 In parallel to all DIC and TA samplings, another set of seawater samples was taken and frozen for
156 measurement of phosphate and silicate concentrations. Total phosphate (precision $0.1 \mu\text{mol kg}^{-1}$)
157 and total silicate (precision $0.2 \mu\text{mol kg}^{-1}$) concentrations were measured using a QuAAtro auto-
158 analyzer with an XY-2 sampler (SEAL Analytical GmbH, Germany).

159 **2.4.1 Correction for Organic Alkalinity**

160 The $p\text{CO}_2$ in the discrete sample was calculated from measured DIC, TA, total phosphate and total
161 silicate using the first and second carbonate system dissociation constants for brackish waters from
162 Millero (2006) and the dissociations constants of HF and HSO_4^- of Perez and Fraga (1987) and
163 Dickson (1990), respectively, with the R package Seacarb (Lavigne and Gattuso, 2013).

164 A critical point for the calculation of carbonate chemistry in waters containing significant amounts
165 of dissolved organic matter, in the following referred to as DOC, is the contribution of organic
166 acid-base components to the TA (Cai et al., 1998; Kuliński et al., 2014 and Yang et al., 2015). This
167 organic TA contribution (TA_{org}) is not reflected in models employed to interpret titration data nor
168 in equations routinely used to perform carbonate system calculations. The classical concept, i.e.
169 two out of four measureable carbonate system parameters are sufficient to calculate the remaining,
170 is limited if TA is one of the measured parameters and the sample contains high amounts of DOC.
171 In such cases, the TA value determined by titration can significantly exceed the amount of TA
172 contributed by the inorganic acid-base components. This hinders an accurate quantification of the
173 inorganic alkalinity and thereby affects the calculation of other carbonate system parameters.



174 Kuliński et al. (2014) demonstrated that the $p\text{CO}_2$ calculated from TA and DIC is typically 100 -
175 200 μatm lower than the measured $p\text{CO}_2$ in open waters of the Baltic Sea. This deviation is not
176 observed if $p\text{CO}_2$ is calculated from measured DIC and pH data (Fig. 2), which are unaffected by
177 the TA_{org} contribution. Two aspects of the present study therefore require the consideration of
178 TA_{org} : (i) TA_{org} explains the observed differences between $p\text{CO}_2$ measured in situ and $p\text{CO}_2$
179 calculated from DIC, TA, silicate and phosphate of discrete samples (Fig. 2) and (ii) TA_{org} needs
180 to be considered when other carbonate system parameters (pH_T , DIC, Ω_{arag} and Ω_{calc}) are calculated
181 from the TA and $p\text{CO}_2$ time series.

182 The offset between measured and calculated $p\text{CO}_2$ caused by TA_{org} increases towards higher $p\text{CO}_2$
183 levels. This could be repeatedly observed during another measuring campaign in Kiel Bay
184 (Hiebenthal et al., 2017, Fig. 2). To furthermore unravel the difference in observed versus
185 calculated $p\text{CO}_2$ for typical Kiel Bay conditions ($S = 16$, $T = 18$ °C, $\text{DOC} = 300$ $\mu\text{mol kg}^{-1}$, $\text{TA} =$
186 1950 $\mu\text{mol kg}^{-1}$), we qualitatively reproduced the impact of TA_{org} on the carbonate system by a
187 modelling approach using regional TA_{org} properties reported by Kuliński et al. (2014). Our
188 modelling approach revealed an offset between measured and observed $p\text{CO}_2$ that increases with
189 CO_2 partial pressure and reaches up to 300 μatm at $p\text{CO}_2$ levels around 2000 μatm (Fig. 2, solid
190 line). A more detailed description of the modelling approach is given in Appendix B.

191 For the calculation of carbonate system parameters (pH , DIC, Ω_{arag} and Ω_{calc}) from TA and $p\text{CO}_2$
192 data, we consequently corrected the TA time series originally based on titration measurements for
193 a TA_{org} contribution. Therefore we used 18 discrete seawater samples taken at 1 m depth right next
194 to a constantly deployed HydroC[®] CO_2 sensor at GEOMAR pier in the inner Kiel Bay, 2 km south
195 of the above described experimental site between March and December 2015 (Hiebenthal et al.,
196 2017). The water samples were poisoned with HgCl_2 (Dickson et al., 2007) within 15 min and
197 stored until measurement of DIC, pH_T and TA at the Leibniz Institute for Baltic Sea Research,
198 Warnemünde, Germany. DIC was analyzed with a SOMMA system at 15 °C. TA was determined
199 by an open-cell titration at 20 °C. Certified reference materials provided by Andrew Dickson's
200 laboratory were measured in parallel for quality assurance. The pH_T of each water sample was
201 determined spectrophotometrically at 25 °C with unpurified m-cresol purple as indicator dye
202 (Hammer et al., 2014). Phosphate and silicate concentrations used for the 2015 samples were



203 measure after Grasshoff 1999 and sampled approximately 240 m from GEOMAR pier (Hiebenthal
204 et al., 2017).

205 The TA_{org} fraction measured in Kiel inner Bay, determined as the difference between TA measured
206 and TA calculated from DIC and pH_T , at GEOMAR pier 2015 was $0.84 \pm 0.0005\%$ (mean \pm SE),
207 corresponding to a contribution between approximately 8 and $30 \mu\text{mol kg}^{-1}$. We chose to consider
208 this conservative range for the carbonate chemistry calculations instead of the values determined
209 during the 2013 deployment, $0.48 \pm 0.28\%$ (mean \pm SE). The reason for using the 2015 value is
210 that it was determined from measurements of TA, DIC and pH_T in the same water samples
211 (Hiebenthal et al., 2017), thereby avoiding the additional uncertainty and noise in the data due to
212 a spatio-temporal mismatch between pCO_2 sensor and discrete sample data of the 2013 field
213 deployment.

214 2.5 Seawater carbonate chemistry

215 We used a model approach based on discrete water sample- and salinity data to estimate total
216 alkalinity (TA) from salinity (S). Given the obvious changes particularly in phosphate and salinity
217 around September 1st (Fig. 3A-B), two separate TA-S regressions were calculated for August and
218 September (Fig. 4, Tab. 1). The slopes and intercepts were used to derive total alkalinity from the
219 salinity time series. Both regressions were highly significant with p-values < 0.001 , $R^2 = 0.64$ and
220 0.92 for August and September respectively and standard deviations of the residuals $< 15 \mu\text{mol}$
221 kg^{-1} (Fig. 4). The two intercepts for August and September are notably different by $100 \mu\text{mol kg}^{-1}$
222 while the two slopes are similar ($\sim 40 \mu\text{mol kg}^{-1}$). An organic-free TA range was calculated
223 (TA_{inorg}) by subtracting constant organic alkalinity contributions of 8 and $30 \mu\text{mol kg}^{-1}$ (lower and
224 upper TA_{org} limits in 2015 measurements at GEOMAR pier; see 2.4) from the TA time series.

225 2.6 Calculation of the regional atmospheric pCO_2

226 Half-hourly measured CO_2 mole fractions in dry air from the German Federal Environment
227 Agency (Umweltbundesamt), Station Westerland, 8.3082°E and 54.9250°N , were averaged for
228 the months August (08th – 31st 2013) and September (01st – 27th 2013): 391 ± 7 and 395 ± 14 ppm
229 (mean \pm SD). Thereof pCO_2 in wet air (100% relative humidity at SST) of 385 and $388 \mu\text{atm}$ for
230 August and September, respectively, were derived at local measurement conditions; i.e. using an
231 averaged sea surface temperature (18.4 ± 0.6 and $16.1 \pm 1.0^\circ\text{C}$) and ambient pressure readings



232 (1019.6 ± 4.2 and 1015.7 ± 7.5 mbar; both parameters from GEOMAR meteorological station,
233 Fig. 1A) as well as the salinity measured in this study (15.6 ± 0.7 and 15.9 ± 1.0).

234 **2.7 Inferential statistics**

235 Daily means, maxima, minima as well as day-night peak-to-peak amplitudes and daily duration of
236 undersaturation for calcite and aragonite (in hours) (mean ± SD) for the months of August and
237 September were compare using Mann-Whitney U tests. Statistical analyses were conducted with
238 Statistica 7 (Statsoft, USA).

239 **3 Results**

240 **3.1 Salinity, water temperature, total silicate and total phosphate observations**

241 Salinity did not show circadian patterns and the daily mean salinity was not significantly different
242 between August and September (Mann-Whitney U, $p > 0.05$, see Appendix C for detailed
243 statistics), with 15.65 ± 0.7 and 15.89 ± 1.01 (mean ± SD), respectively (Fig. 3A). The total
244 alkalinity (TA), derived from salinity, varied between 1934 and 1956 $\mu\text{mol kg}^{-1}$ during the 2
245 months, with a SD of 41 $\mu\text{mol kg}^{-1}$. As a marker of seasonality, temperature daily means, minima,
246 maxima were all significantly lower in September compared to August (Mann-Whitney U, $p <$
247 0.001 , see Appendix C), with drops of 2.3 °C, 2.2 °C and 3 °C, respectively (Tab. 2, Fig. 3A, 4A).
248 The daily variation amplitude was significantly reduced in September by 0.3°C compared to
249 August (Mann-Whitney U, $p < 0.01$, see Appendix C). Total silicate was not significantly different
250 between August and September: $19.0 \pm 4.9 \mu\text{mol kg}^{-1}$ and $18.8 \pm 5.4 \mu\text{mol kg}^{-1}$ (Mann-Whitney
251 U, $p > 0.05$, see Appendix C). Total phosphate was significantly different between August and
252 September: $0.7 \pm 0.14 \mu\text{mol kg}^{-1}$ and $5.9 \pm 3.7 \mu\text{mol kg}^{-1}$ (Mann-Whitney U, $p < 0.001$, see
253 Appendix C).

254 **3.2 $p\text{CO}_2$ and $[\text{O}_2]$ observations**

255 The daily mean (± SD) $p\text{CO}_2$ of $628 \pm 114 \mu\text{atm}$ in August and $652 \pm 193 \mu\text{atm}$ in September (Tab.
256 2) remained always above the regional atmospheric $p\text{CO}_2$ of approximately 387 μatm . The mean
257 daily minimum and maximum $p\text{CO}_2$ values were $334 \pm 119 \mu\text{atm}$ and $1151 \pm 328 \mu\text{atm}$ in August
258 and $373 \pm 139 \mu\text{atm}$ and $1097 \pm 336 \mu\text{atm}$ (mean ± SD) in September, respectively (see Tab. 2,



259 Figs. 3C, 5B). A modest and non-significant increase of the daily means was observed between
260 August and September (+ 22 μatm) as well as a non-significant average decrease of the day-night
261 variability by 93 μatm (Mann-Whitney U, $p > 0.05$, see Appendix C) (Tab. 2). A high $p\text{CO}_2$ event
262 was observed between September 8th and September 12th with a peak of the daily mean $p\text{CO}_2$ to
263 1166 μatm on September 9th. On this day, a maximum $p\text{CO}_2$ of 1839 μatm was observed at
264 04:30 a.m. (see Fig. 3C).

265 The daily mean $[\text{O}_2]$ most of the time remained below the seawater saturation threshold (~ 260 to
266 290 $\mu\text{mol kg}^{-1}$) (Fig. 3D, Tab. 2). However, supersaturation due to photosynthesis was regularly
267 observed between noon and sunset in August. Significant decreases of the daily average, maximum
268 and minimum $[\text{O}_2]$ by 47 $\mu\text{mol kg}^{-1}$, 64 $\mu\text{mol kg}^{-1}$, 35 $\mu\text{mol kg}^{-1}$, respectively, were observed in
269 September (Mann-Whitney U, all $p < 0.001$, see Appendix C for details) (Tab. 2, Fig. 5C), with
270 an abrupt $[\text{O}_2]$ decrease occurring on Sept. 8th, in parallel to a sudden decrease in temperature by
271 approximately 2 °C (Fig. 3A-D). A significant decrease of the day-night amplitude by 29 $\mu\text{mol kg}^{-1}$
272 was observed from August to September (Mann-Whitney U, $p = 0.008$, Appendix C). The
273 threshold for hypoxia (60 $\mu\text{mol kg}^{-1}$) is never undercut (see Fig. 3D); the minimum daily mean
274 concentration observed during the two months was 140 $\mu\text{mol kg}^{-1}$.

275 3.3 Derived carbonate chemistry parameters

276 Times series for pH_T , DIC, Ω_{arag} and Ω_{calc} (Fig. 6) were derived from modeled TA_{inorg} (Fig. 4) and
277 measured $p\text{CO}_2$ and analyzed for daily means, minima, maxima and diel peak-to-peak amplitudes
278 (mean \pm SD) with $\text{TA}_{\text{org}} = 8 \mu\text{mol kg}^{-1}$ and $\text{TA}_{\text{org}} = 30 \mu\text{mol kg}^{-1}$ (Tab. 1). Since the differences in
279 the calculated parameters between the $\text{TA}_{\text{org}} = 8 \mu\text{mol kg}^{-1}$ and the $\text{TA}_{\text{org}} = 30 \mu\text{mol kg}^{-1}$ estimates
280 are too small to be recognizable in Fig. 6, only results for the mean $\text{TA}_{\text{org}} = 19 \mu\text{mol kg}^{-1}$ are
281 shown. Overall, we observe a slight and non-significant (Mann-Whitney U, $p > 0.05$, see Appendix
282 C for details) decrease in daily means of DIC and pH_T between August and September by 11 μmol
283 kg^{-1} and 0.02 pH_T units respectively (Tab. 1). In parallel, we observe a non-significant decrease of
284 the amplitudes of the diel variations in DIC of 21 $\mu\text{mol kg}^{-1}$ (Mann-Whitney U, $p > 0.05$, see
285 Appendix C) and pH_T of approximately 0.05 pH_T units (Mann-Whitney U, $p > 0.05$, see Appendix
286 C) and (Tab. 1, Fig. 5). All these observations are coherent with the changes in $p\text{CO}_2$ previously
287 described.



288 Daily means of Ω_{arag} are close to the saturation threshold: between 1.3 and 1.4 in August and 1.2
289 in September (Tab. 1). For both, Ω_{arag} and Ω_{calc} , we observe a significant decrease in daily mean
290 values (Mann-Whitney U, all $p < 0.01$, see Appendix C) and a marginally significant decrease of
291 diel amplitudes between August and September (Mann-Whitney U, all $p < 0.1$, see Appendix C)
292 (Tab. 1, Fig. 5). In both isoforms, the amplitudes decrease results from a significant reduction of
293 the daily maxima (Mann-Whitney U, $p = 0.001$, see Appendix C) with the minima remaining
294 constant (Mann-Whitney U, $p > 0.05$, see Appendix C) (Tab. 1, Fig. 5). On average, the seawater
295 was undersaturated with respect to aragonite for approximately 6 hours per days in August and
296 approximately 9 hours per day in September (Tab. 1). Similarly, seawater was undersaturated with
297 respect to calcite for approximately 30 min and approximately 1 hour 30 min in August and
298 September, respectively (Tab. 1). Only one full day of undersaturation with respect to aragonite
299 was observed on September 9th during the high $p\text{CO}_2$ event (Fig. 5).

300 Over the whole measurement period, the consideration of organic alkalinity contributions has little
301 effect on the derived CO_2 system parameters (mean value differences: $20 \mu\text{mol kg}^{-1}$ DIC, $< 2 \mu\text{mol}$
302 kg^{-1} $[\text{CO}_3^{2-}]$ and negligible effect on omegas and pH_T). The only noticeable difference when taking
303 TA_{org} into account was an increase of time of undersaturation for Ω_{arag} and Ω_{calc} in September of
304 approximately 25 min and approximately 10 min, respectively.

305 4 Discussion

306 4.1 $p\text{CO}_2$, carbonate chemistry and O_2

307 Monthly averages of $p\text{CO}_2$ close to the seafloor as presented in this study ($\sim 640 \mu\text{atm}$; Tab. 1)
308 were more than 50% above atmospheric $p\text{CO}_2$. In 2011, Saderne et al. (2013), used similar
309 technologies as in our study in a seaweed dominated bed of Eckernförde Bay (adjacent to Kiel
310 Bay, Western Baltic) and found significantly lower weekly mean $p\text{CO}_2$ values ($\sim 390 \mu\text{atm}$ in July,
311 $\sim 240 \mu\text{atm}$ in August and $420 \mu\text{atm}$ in September, excluding an upwelling event, Saderne et al.,
312 2013). Accordingly, the day-night amplitudes of $p\text{CO}_2$ observed in the present study (764 ± 310
313 μatm , overall mean \pm SD) are 3 to 4 times higher than observed during “normal” days by Saderne
314 et al. (2013) ($243 \pm 95 \mu\text{atm}$) in the neighboring Eckernförde Bay in 2011. This reflects a
315 characteristic of the marine carbonate system: Equal DIC variations will induce stronger $p\text{CO}_2$
316 variations at high “baseline” $p\text{CO}_2$ levels compared to lower $p\text{CO}_2$ levels. The source of this pattern



317 is the reduced buffering capacity of the carbonate system at a high $p\text{CO}_2$ “baseline”. Accordingly,
318 Saderne et al. (2013) found extreme $p\text{CO}_2$ variations of approximately 1700 μatm during an
319 upwelling event that lifted the “baseline” $p\text{CO}_2$ to approximately 1600 μatm , although the DIC
320 variations due to plant photosynthesis remained rather unchanged by the upwelling. Likewise, the
321 amplitude of the diel DIC variations during our study (145 $\mu\text{mol kg}^{-1}$ in August and 124 $\mu\text{mol kg}^{-1}$
322 in September, see Tab.1 and Fig. 5) were of the same magnitude as what had been observed in
323 Eckernförde Bay before and after upwelling (141 $\mu\text{mol kg}^{-1}$ and 106 $\mu\text{mol kg}^{-1}$,
324 respectively, Saderne et al., 2013).

325 Average O_2 concentrations were below saturation in August and September 2013, with a
326 significant decrease occurring in September (monthly means of 89.4% $[\text{O}_2]_{\text{sat}}$ and 68.8% $[\text{O}_2]_{\text{sat}}$
327 for August and September respectively). However, we note that at no point of our survey the
328 threshold of hypoxia (~22% saturation; 60 $\mu\text{mol kg}^{-1}$) was reached. The significant O_2 decrease in
329 September co-occurred with an increase in phosphate and a change in DIC to TA regression. This
330 can possibly be explained by a rapid degradation of the seagrass shoots observed in September and
331 a possible shift of the habitat from an auto- to a heterotrophic system.

332 4.2 Implications for mussel calcification in a seagrass meadow

333 We found pronounced variations of Ω_{calc} and Ω_{arag} on a daily basis, e.g., resulting in 5.7 to 8.8 h
334 of undersaturation for aragonite per day in the water body right above the mussel patch.

335 As expected, daytime photosynthesis counters water corrosiveness caused by heterotrophic
336 processes, while at night water corrosiveness is reinforced by respiration. Waldbusser et al. (2014)
337 demonstrated that saturation states (and therefore $[\text{CO}_3^{2-}]$) are the parameters affecting the larval
338 development and growth of *Mytilus galloprovincialis* and *Crassostrea gigas*. On young *M. edulis*
339 Hiebenthal et al. (2013) found a negative correlation between growth and Ω or $[\text{CO}_3^{2-}]$. Thomsen
340 et al. (2015) confirmed these findings in larvae and juveniles. With a meta-analysis including all
341 past work on mussel populations from Kiel Bay, they found that the critical CO_3^{2-} concentration
342 below which calcification starts to decline was 80 $\mu\text{mol kg}^{-1}$ (although they specified that the
343 directly related ratio $[\text{H}^+]/[\text{HCO}_3^-]$ is likely to be the controlling parameter for calcification,
344 Thomsen et al. 2015). In our survey, mussels were exposed to $[\text{CO}_3^{2-}]$ below this threshold for 12
345 ± 5.2 h per day in August and 15.3 ± 5.4 h per day in September (mean \pm SD). Comparing these



346 findings to the shorter durations of aragonite (5-9 h per day) and calcite (~1 h per day)
347 undersaturation implies that reduced calcification rates might already occur during periods with
348 low, yet oversaturated calcium carbonate concentrations. However, the consequences of these
349 successions of intense corrosive stress and stress relaxation on the juvenile and adults forming the
350 mussel patch is still under debate. On mussel larvae, Frieder et al., 2013 showed that the negative
351 effects of elevated $p\text{CO}_2$ (~1500 μatm) on *Mytilus galloprovincialis* disappear, if diel variations
352 of 500 μatm were added, although this effect was not observed for *Mytilus californianus*. Wahl et
353 al. (2017) found that in laboratory and mesocosm experiments calcification of blue mussels is
354 significantly higher during daytime, when photosynthetic activity of macrophytes creates
355 favorable calcification conditions. However, in field studies they did not detect a positive net effect
356 of the co-occurrence with macrophytes on the calcification of mussels (Wahl et al. 2017).
357 Furthermore, Thomsen et al. (2013) showed that high food availability, particularly in Kiel Bay,
358 can circumvent the effects of acidification in mussels.

359

360 **Conclusion**

361 Our study demonstrates how essential it is to place more effort in measuring the carbonate
362 chemistry variations in nearshores habitats, and highlights the need to include variability when
363 investigating the impact of OA on benthic organisms. We emphasize that continuous carbonate
364 system observations in benthic habitats are possible but challenging due to the high spatio-
365 temporal variability and organic alkalinity contributions. However, with the here applied
366 combination of in situ sensor measurements, laboratory analyses of discrete water samples, and
367 modelling elements we were able to distinguish daily oscillations and shifts of averages (across
368 weeks) of several seawater chemistry parameters. This approach specifically allowed for a
369 temporal quantification of dissolution threshold undercuts *M. edulis* experiences in this exemplary
370 site of Kiel Bay.

371 **Appendix A: HydroC[®] response time and related signal processing**

372 The entire HydroC[®] $p\text{CO}_2$ time series has a total of 187 zeroings and related flush intervals. A first
373 order kinetics model was fitted to every of the HydroC[®]'s signal recoveries from its zero value to
374 ambient partial pressure over an 55 min flush interval to obtain sensor response times (see Fiedler



375 et al. 2013). The fit interval was set to extend over 55 min to be around 6 times as large as the
376 sensor's response time to allow for reasonable fitting of the exponential increase. In general the
377 carbonate system at the site was characterized by a strongly varying baseline featuring very steep
378 $p\text{CO}_2$ gradients over the course of the day with slopes of up to $-54 \mu\text{atm}/\text{min}$. Therefore the $p\text{CO}_2$
379 signal recovery from zero to ambient during the 187 flush intervals was often superimposed with
380 a changing background partial pressure. These adverse conditions hamper the response time
381 determination by means of a first order kinetics fit. We therefore flagged and not considered further
382 the recoveries providing the worst fit results, which indicates a bad match between model and real
383 signal: (i) the fits characterized by the largest 10% of root mean square (RMS) residuals of the
384 fitted curve and the real signal as well as (ii) the fits with the largest 10% of the uncertainty of the
385 fitted response time.

386 Finally a total of 157 fit results were considered providing an average response time (t_{63}) of
387 $546 \pm 208 \text{ s}$ with an RMS of the fit function of $6.0 \pm 3.1 \mu\text{atm}$ and a fit uncertainty for the response
388 time of $1.2 \pm 0.4 \text{ s}$. The average response time found is in good agreement with a t_{63} of
389 $553 \pm 8 \mu\text{atm}$ as determined during a dedicated laboratory test with a similar sensor setup at 14.5°C
390 water temperature. The large standard deviation of the averaged in situ response times (i.e. 208 s)
391 is likely caused (i) by the influence of the strongly varying background $p\text{CO}_2$ on the data to be
392 fitted and (ii) by the variability of the water exchange in front of the membrane within the flow-
393 head as caused by i.e. changes in the ambient water currents. Against the large variability in the
394 determined response times, a temperature dependence of the t_{63} can be neglected as well as a
395 potential response deceleration caused by fouling on the membrane, which was only observed to
396 a very small extend after the deployment.

397 The response time (RT) correction according to Miloshevich et al. (2004) and Fiedler et al. (2013)
398 was carried out with a constant response time of 546 s to obtain the final $p\text{CO}_2$ series. The $p\text{CO}_2$
399 data were additionally RT-corrected with a reduced ($\text{RT}_{\text{short}} = 546 - 208 = 338 \text{ s}$) and an extended
400 response time ($\text{RT}_{\text{long}} = 546 + 208 = 754 \text{ s}$). In order to estimate the uncertainty of the final $p\text{CO}_2$
401 time series, the differences between the RT_{long} - and the RT-corrected as well as between the RT-
402 and the RT_{short} -corrected $p\text{CO}_2$ time series were determined. They both provide a small average
403 $\Delta p\text{CO}_2$ of $0.8 \mu\text{atm}$ (0.06% of reading) and a corresponding standard deviation of $10 \mu\text{atm}$ (1.5%
404 of reading). The standard deviation is influenced by short periods characterized by large $p\text{CO}_2$
405 gradients where the RT-correction has the largest effect; i.e. at $130 \mu\text{atm}/\text{min}$ over 3 minutes



406 (54 $\mu\text{atm}/\text{min}$ in the original, non-RT-corrected data) the steepest $p\text{CO}_2$ decline of the series was
407 observed in the early morning of August 22nd at around 4:40 causing the maximum observed
408 individual $\Delta p\text{CO}_2$ of $-172 \mu\text{atm}$ or 23% of reading.

409 The standard deviation of the $\Delta p\text{CO}_2$ (1.5% of reading) is used as a measure for the $p\text{CO}_2$
410 uncertainty in this study related to the response time influences. Not considering the response time
411 and applying a related correction, would have forced us to continue the analysis with a less
412 realistic, “smoothed” data set that showed temporally delayed as well as amplitude-damped $p\text{CO}_2$
413 peaks and troughs.

414 Fiedler, B., Fietzek, P., Vieira, N., Silva, P., Bittig, H. C. and Körtzinger, A.: In Situ CO_2 and O_2
415 Measurements on a Profiling Float, J. Atmos. Ocean. Technol., 30(1), 112–126,
416 doi:10.1175/JTECH-D-12-00043.1, 2013.

417 Miloshevich, L. M., Paukkunen, A., Vömel, H. and Oltmans, S. J.: Development and validation of
418 a time-lag correction for Vaisala radiosonde humidity measurements, J. Atmos. Ocean. Technol.,
419 21(9), 1305–1327, 2004.

420 **Appendix B**

421 We implemented a model to estimate the potential error associated to CO_2 system calculations, in
422 case one of the input parameters is titrated TA including organic acid-base components.

423 Hence, we firstly calculated the carbonate system at varying DIC and constant TA, salinity, and
424 temperature. In this case the derived carbonate system parameters (i.e. $p\text{CO}_2$) reflect values as
425 calculated from TA and DIC measured in discrete samples.

426 Organic contribution to TA (TA_{org}) is estimated based on the relation reported by Kuliński et al.
427 (2014) for the Baltic Sea, which approximates TA_{org} from the proton concentration $[\text{H}^+]$, the
428 amount of DOC, a bulk dissociation constant (K_{DOM}) and the fraction of DOC (f) acting as a carrier
429 of weakly acidic groups

$$430 \quad \text{TA}_{\text{org}} = \frac{K_{\text{DOM}} \cdot f \cdot \text{DOC}}{[\text{H}^+] + K_{\text{DOM}}}$$

431 This TA_{org} estimate is a side-specific approximation since K_{DOM} and f ($2.94 \times 10^{-8} \text{ mol kg}^{-1}$ and
432 0.14, respectively) are characteristic for the actual DOM composition. Further, K_{DOM} is currently
433 only reported for $T=25^\circ\text{C}$ and no salinity-dependence was investigated. Therefore, this model is
434 only a qualitative approximation of the carbonate system in high DOC waters.



435 The inorganic TA fraction can be approximated as $TA_{inorg} = TA - TA_{org}$. This TA_{inorg} together with
 436 DIC can be used to calculate the “correct” pCO_2 ($pCO_{2,sensor}$) as it would also be obtained from
 437 direct observations, since TA_{inorg} represents the share of the alkalinity which is covered by the
 438 dissociation constants and equilibrium reactions implemented in the routinely applied carbonate
 439 system models (i.e. CO_{2sys} , seacarb).

440 Finally, the TA_{org} estimate needs to be refined. Above, it was estimated from the proton
 441 concentration, which itself was derived from TA and DIC. Now, TA_{inorg} is the better input
 442 parameter to calculate this proton concentration. Thus, we recalculate first TA_{org} to get a refined
 443 value ($TA_{org,ref}$). The other carbonate system parameters, including $pCO_{2,sensor,ref}$, are calculated
 444 with $TA_{org,ref}$. This refinement procedure was repeated iteratively, until no significant changes
 445 occurred between the iterative steps. The finally obtained $pCO_{2,sensor,ref}$ would reflect direct pCO_2
 446 measurements performed with a dedicated in situ sensor.

447 Model output:

448 The model predicts an increase in the deviation between pCO_2 measured in situ ($pCO_{2,sensor,ref}$) and
 449 pCO_2 values obtained by calculations from discrete sample TA and DIC towards pCO_2 levels
 450 around 2000 μatm as depicted in Fig. 2 (input parameters: $S = 16$, $T = 18$ °C, $DOC = 300$ μmol
 451 kg^{-1} , $TA = 1950$ μmol kg^{-1} , K_{DOM} and f from Kuliński et al. (2014), CO_2 system constants from
 452 Millero et al. (2006)).

453 Kuliński, K., Schneider, B., Hammer, K., Machulik, U. and Schulz-Bull, D.: The influence of
 454 dissolved organic matter on the acid–base system of the Baltic Sea, *J. Mar. Syst.*, 132, 106–115,
 455 doi:10.1016/j.jmarsys.2014.01.011, 2014.

456 Millero, F. J., Graham, T. B., Huang, F., Bustos-Serrano, H. and Pierrot, D.: Dissociation constants
 457 of carbonic acid in seawater as a function of salinity and temperature, *Mar. Chem.*, 100(1-2), 80–
 458 94, doi:10.1016/j.marchem.2005.12.001, 2006.

459

460 Appendix C: Mann-Whitney U tests details

461 Result table for the Mann Whitney tests comparing August and September data listed in Table 2.

	U	Z	p-value	August n	September n
Mean Temperature	2	5.71	<0.01	20	26
Min. Temperature	5	5.64	<0.01	20	26
Max. Temperature	1	5.73	<0.01	20	26
Δ Temperature	133	2.80	0.01	20	26



Mean Salinity	198	-1.36	0.17	20	26
Min. Salinity	196	-1.41	0.16	20	26
Max. Salinity	186	-1.63	0.10	20	26
Δ Salinity	252	-0.17	0.87	20	26
Total Silicate	114	0.100	0.920	13	18
Total Phosphate	0	-4.665	<0.001	13	18
Mean $p\text{CO}_2$	255	0.10	0.92	20	26
Min. $p\text{CO}_2$	220	-0.88	0.38	20	26
Max. $p\text{CO}_2$	233	0.59	0.56	20	26
$\Delta p\text{CO}_2$	220	0.88	0.38	20	26
Mean $[\text{O}_2]$	67	4.758	<0.001	24	26
Min. $[\text{O}_2]$	121	3.709	<0.001	24	26
Max. $[\text{O}_2]$	68	4.738	<0.001	24	26
$\Delta[\text{O}_2]$	176	2.641	0.008	24	26
$\text{TA}_{\text{org}} = 8$					
	U	Z	p-value	August n	September n
Mean pH_T	241	0.41	0.68	20	26
Min. pH_T	246	-0.30	0.76	20	26
Max. pH_T	212	1.05	0.29	20	26
ΔpH_T	215	0.99	0.32	20	26
Mean DIC	254	0.12	0.90	20	26
Min. DIC	227	-0.72	0.47	20	26
Max. DIC	203	1.25	0.21	20	26
Δ DIC	198	1.36	0.17	20	26
Mean $[\text{CO}_3^{2-}]$	172	1.94	0.05	20	26
Min. $[\text{CO}_3^{2-}]$	225	0.76	0.44	20	26
Max. $[\text{CO}_3^{2-}]$	153	2.36	0.02	20	26
$\Delta[\text{CO}_3^{2-}]$	181	1.74	0.08	20	26
Mean Ω_{arag}	157	2.27	0.02	20	26
Min. Ω_{arag}	213	1.03	0.30	20	26
Max. Ω_{arag}	150	2.43	0.02	20	26
$\Delta \Omega_{\text{arag}}$	176	1.85	0.06	20	26
time $\Omega_{\text{arag}} < 1$	176	-1.85	0.06	20	26
Mean Ω_{calc}	167	2.05	0.04	20	26
Min. Ω_{calc}	215	0.99	0.32	20	26
Max. Ω_{calc}	152	2.38	0.02	20	26



$\Delta \Omega_{\text{calc}}$	178	1.81	0.07	20	26
time $\Omega_{\text{calc}} < 1$	212	-1.05	0.29	20	26
TA _{org} = 30					
	U	Z	p-value	August n	September n
Mean pH _T	241	0.41	0.68	20	26
Min. pH _T	246	-0.30	0.76	20	26
Max. pH _T	212	1.05	0.29	20	26
Δ pH _T	215	0.99	0.32	20	26
Mean DIC	253	0.14	0.89	20	26
Min. DIC	228	-0.70	0.49	20	26
Max. DIC	203	1.25	0.21	20	26
Δ DIC	197	1.38	0.17	20	26
Mean [CO ₃ ²⁻]	172	1.94	0.05	20	26
Min. [CO ₃ ²⁻]	225	0.76	0.44	20	26
Max. [CO ₃ ²⁻]	151	2.40	0.02	20	26
Δ [CO ₃ ²⁻]	181	1.74	0.08	20	26
Mean Ω_{arag}	157	2.27	0.02	20	26
Min. Ω_{arag}	213	1.03	0.30	20	26
Max. Ω_{arag}	149	2.45	0.01	20	26
$\Delta \Omega_{\text{arag}}$	176	1.85	0.06	20	26
time $\Omega_{\text{arag}} < 1$	175	-1.87	0.06	20	26
Mean Ω_{calc}	168	2.03	0.04	20	26
Min. Ω_{calc}	214	1.01	0.31	20	26
Max. Ω_{calc}	152	2.38	0.02	20	26
$\Delta \Omega_{\text{calc}}$	178	1.81	0.07	20	26
time $\Omega_{\text{calc}} < 1$	218	-0.9	0.4	20	26

462

463 Acknowledgements

464 The authors would like to thank particularly Dr. Todd Martz and his team from the Scripps
 465 Institution of Oceanography (San Diego, USA) for providing the salinity / [O₂] / T° sensor package
 466 and for their precious technical assistance. We also wish to thank the Kiel Marine Organism
 467 Culture Centre (KIMOCC) of the Kiel Cluster of excellence “Future Ocean”; Sebastian Fessler
 468 from GEOMAR for the TA / DIC sample measurements; Dr. Bernd Schneider and Stefan Bucker



469 from the IOW are thanked for valuable discussions with respect to carbonate system analysis in
470 the Baltic Sea as well as for the inter comparison between TA / DIC / pH measurements; Prof.
471 Peter Herman from the NIOZ Royal Netherlands Institute for Sea Research for providing access
472 to the nutrient analyzer; Dr. Jörn Thomsen for his comments on the manuscript; the research divers
473 from GEOMAR among which are Prof. Martin Wahl, Dr. Christian Pansch, Dr. Yvonne Sawall
474 and Christian Lieberum; the personnel of the “Seebar am Seebad Düsternbrook” restaurant for
475 providing electricity to the sensors as well as the Kiel early morning nudist club for its cooperation
476 in providing access to the Seebar. This work has been funded by the Kiel Cluster of excellence
477 “Future Ocean”.

478



479 **References**

480 Andersson, A. J., Mackenzie, F. T. and Gattuso, J.-P.: Effects of ocean acidification on benthic
481 processes, organisms, and ecosystems, in Ocean Acidification, p. xix, 326 p., 2011.

482 Bates, N. R., Y. M. Astor, M. J. Church, and others. 2014. A time-series view of changing surface
483 ocean chemistry due to ocean uptake of anthropogenic CO₂ and ocean acidification. *Oceanography*
484 27: 126–141. doi:<http://dx.doi.org/10.5670/oceanog.2014.16>Cai, W.-J., Y. Wang, and R. E.
485 Hodson: Acid-Base Properties of Dissolved Organic Matter in the Estuarine Waters of Georgia,
486 USA. *Geochim. Cosmochim. Acta* 62: 473–483. doi:10.1016/S0016-7037(97)00363-3, 1998.

487 Cai, W.-J., Wang, Y., and Hodson, R. E.: Acid-base properties of dissolved organic matter in the
488 estuarine waters of Georgia, USA, *Geochim. Cosmochim. Ac.*, 62, 473–483, 1998

489 Diaz, R. J. and Rosenberg, R.: Spreading dead zones and consequences for marine ecosystems.,
490 *Science*, 321(5891), 926–9, doi:10.1126/science.1156401, 2008.

491 Dickson, A. G.: Standard potential of the reaction: $\text{AgCl(s)} + \frac{1}{2} \text{H}_2\text{(g)} = \text{Ag(s)} + \text{HCl(aq)}$, and the
492 standard acidity constant of the ion HSO_4^- in synthetic sea water from 273.15 to 318.15 K, *J. Chem.*
493 *Thermodyn.*, 22(2), 113–127, doi:10.1016/0021-9614(90)90074-Z, 1990.

494 Dickson, A. G., Sabine, C. L. and Christian, J. R.: Guide to Best Practices for Ocean CO₂
495 Measurements, PICES spec., 2007.

496 Doney, S. C., V. J. Fabry, R. A. Feely, and J. A. Kleypas. 2009. Ocean Acidification: The Other
497 CO₂ Problem. *Ann. Rev. Mar. Sci.* 1: 169–192. doi:10.1146/annurev.marine.010908.163834

498 Duarte, C. M., Hendriks, I. E., Moore, T. S., Olsen, Y. S., Steckbauer, A., Ramajo, L., Carstensen,
499 J., Trotter, J. A. and McCulloch, M.: Is Ocean Acidification an Open-Ocean Syndrome?
500 Understanding Anthropogenic Impacts on Seawater pH, *Estuaries and Coasts*, 36(2), 221–236,
501 doi:10.1007/s12237-013-9594-3, 2013.

502 Feely, R. A., Sabine, C. L., Hernandez-Ayon, J. M., Ianson, D. and Hales, B.: Evidence for
503 upwelling of corrosive "acidified" water onto the continental shelf, *Science*, 320, 1490-1492, 2008.



- 504 Fietzek, P., Fiedler, B., Steinhoff, T. and Körtzinger, A.: In situ quality assessment of a novel
505 underwater pCO₂ sensor based on membrane equilibration and NDIR spectrometry, *J. Atmos.*
506 *Ocean. Technol.*, 31(1), 181–196, 2014.
- 507 Frieder, C. A., Gonzalez, J. P., Bockmon, E. E., Navarro, M. O. and Levin, L. A.: Can variable pH
508 and low oxygen moderate ocean acidification outcomes for mussel larvae?, *Glob. Chang. Biol.*, 1–
509 11, doi:10.1111/gcb.12485, 2013.
- 510 Geomar, Helmholtz Center for Ocean Research Kiel. Available from:
511 <http://www.geomar.de/service/wetter/>
- 512 Grasshoff, K., Kremling, K. and Ehrhardt, M.G.: *Methods of Seawater Analysis* (3rd Edition).
513 VCH Publishers. 632 pp, 1999.
- 514 Hammer, K., Schneider, B., Kuliński, K. and Schulz-Bull, D. E.: Precision and accuracy of
515 spectrophotometric pH measurements at environmental conditions in the Baltic Sea, *Estuar. Coast.*
516 *Shelf Sci.*, 146, 24–32, 2014.
- 517 Harvey, B. P., Gwynn-Jones, D. and Moore, P. J.: Meta-analysis reveals complex marine
518 biological responses to the interactive effects of ocean acidification and warming, *Ecol. Evol.*, 3,
519 1016–1030, doi:10.1002/ece3.516, 2013.
- 520 Hiebenthal, C., Philipp, E. E. R., Eisenhauer, A. and Wahl, M.: Effects of seawater pCO₂ and
521 temperature on shell growth, shell stability, condition and cellular stress of Western Baltic Sea
522 *Mytilus edulis* (L.) and *Arctica islandica* (L.), *Mar. Biol.*, 160(2013), 2073–2087,
523 doi:10.1007/s00227-012-2080-9, 2013.
- 524 Hiebenthal, C., Fietzek, P., Müller, J.D., Otto, S., Rehder, G., Paulsen, M., Stuhr, A., Clemmesen-
525 Bockelmann, C., Melzner, F.: Kiel fjord carbonate chemistry data between 2015 (February) and
526 2016 (January). GEOMAR - Helmholtz Centre for Ocean Research Kiel, Pangea Dataset #876551
527 (DOI registration in progress), 2017.
- 528 Hofmann, G. E., Smith, J. E., Johnson, K. S., Send, U., Levin, L. A., Micheli, F., Paytan, A., Price,
529 N. N., Peterson, B., Takeshita, Y., Matson, P. G., Crook, E. D., Kroeker, K. J., Gambi, M. C.,
530 Rivest, E. B., Frieder, C. A., Yu, P. C. and Martz, T. R.: High-frequency dynamics of ocean pH: a



- 531 multi-ecosystem comparison., *PLoS One*, 6(12), e28983, doi:10.1371/journal.pone.0028983,
532 2011.
- 533 Keeling, R. F., Körtzinger, A. and Gruber, N.: Ocean Deoxygenation in a Warming World, *Ann.*
534 *Rev. Mar. Sci.*, 2(1), 199–229, doi:10.1146/annurev.marine.010908.163855, 2010.
- 535 Kögler, F.-C. and Ulrich, J., *Bodengestalten und Sedimente der Kieler Förde*, *Schr. Naturwiss.*
536 *Ver. Schleswig-Holstein*, 55, 1–33, 1985.
- 537 Kuliński, K., Schneider, B., Hammer, K., Machulik, U. and Schulz-Bull, D.: The influence of
538 dissolved organic matter on the acid–base system of the Baltic Sea, *J. Mar. Syst.*, 132, 106–115,
539 doi:10.1016/j.jmarsys.2014.01.011, 2014.
- 540 Lavigne, H. and Gattuso, J.-P.: seacarb: seawater carbonate chemistry with R. R package version
541 2.3. 3, Software [online] Available from:
542 [http://scholar.google.com/scholar?hl=en&btnG=Search&q=intitle:seacarb:+seawater+carbonate+](http://scholar.google.com/scholar?hl=en&btnG=Search&q=intitle:seacarb:+seawater+carbonate+chemistry+with+R.+R+package+version+2.3#0)
543 [chemistry+with+R.+R+package+version+2.3#0](http://scholar.google.com/scholar?hl=en&btnG=Search&q=intitle:seacarb:+seawater+carbonate+chemistry+with+R.+R+package+version+2.3#0), 2010.
- 544 Melzner, F., Thomsen, J., Koeve, W., Oeschlies, A., Gutowska, M. A., Bange, H. W., Hansen, H.
545 P. and Körtzinger, A.: Future ocean acidification will be amplified by hypoxia in coastal habitats,
546 *Mar. Biol.*, 16, 1875–1888, doi:10.1007/s00227-012-1954-1, 2012.
- 547 Millero, F. J., Graham, T. B., Huang, F., Bustos-Serrano, H. and Pierrot, D.: Dissociation constants
548 of carbonic acid in seawater as a function of salinity and temperature, *Mar. Chem.*, 100(1-2), 80–
549 94, doi:10.1016/j.marchem.2005.12.001, 2006.
- 550 Müller, J. D., B. Schneider, and G. Rehder. 2016. Long-term alkalinity trends in the Baltic Sea and
551 their implications for CO₂-induced acidification. *Limnol. Oceanogr.* 61: 1984–2002.
552 doi:10.1002/LNO.10349
- 553 NOAA - ESRL, Available from: <http://www.esrl.noaa.gov/gmd/ccgg/trends>, 2014.
- 554 Orr, J. C., Fabry, V.J., Aumont, O., Bopp, L., Doney, S.C., Feely, R. A., Gnanadesikan, A., Gruber,
555 N., Ishida, A., Joos, F., Key, R. M., Lindsay, K., Maier-Reimer, E., Matear, R., Monfray, P.,
556 Mouchet, A., Najjar, R.G., Plattner, G.K., Rodgers, K.B., Sabine, C.L., Sarmiento, J.L., Schlitzer,
557 R., Slater, R.D., Totterdell, I.J., Weirig, M.F., Yamanaka, Y. and Yool, A.: Anthropogenic ocean



558 acidification over the twenty-first century and its impact on calcifying organisms, *Nature*, 437,
559 681–686, 2005.

560 Perez, F. F. and Fraga, F.: The pH measurements in seawater on the NBS scale, *Mar. Chem.*, 21,
561 315–327, 1987.

562 Reusch, T. B. H. and Chapman, A. R. O.: Storm effects on eelgrass (*Zostera marina* L.) and blue
563 mussel (*Mytilus edulis* L.) beds, *J. Exp. Mar. Bio. Ecol.*, 192(2), 257–271, doi:10.1016/0022-
564 0981(95)00074-2, 1995.

565 Saderne, V., Fietzek, P. and Herman, P. M. J.: Extreme Variations of pCO₂ and pH in a Macrophyte
566 Meadow of the Baltic Sea in Summer: Evidence of the Effect of Photosynthesis and Local
567 Upwelling, *PLoS One*, 8(4), e62689, doi:10.1371/journal.pone.0062689, 2013.

568 Schwarzer, K. and Themann, S.: Sediment distribution and geological buildup of Kiel Bay
569 (Western Baltic Sea), *Meyniana*, 55, 91–115, 2003.

570 Thomsen, J., Casties, I., Pansch, C., Körtzinger, A. and Melzner, F.: Food availability outweighs
571 ocean acidification effects in juvenile *Mytilus edulis*: laboratory and field experiments, *Glob.*
572 *Change Biol.*, 19, 1017–1027, doi:10.1111/gcb.12109, 2013,

573 Thomsen, J., Haynert, K., Wegner, K. M. and Melzner, F.: Impact of seawater carbonate chemistry
574 on the calcification of marine bivalves, *Biogeosciences Discuss.*, 12(2), 1543–1571,
575 doi:10.5194/bg-12-1543-2015, 2015.

576 Vinther, H. F. and Holmer, M.: Experimental test of biodeposition and ammonium excretion from
577 blue mussels (*Mytilus edulis*) on eelgrass (*Zostera marina*) performance, *J. Exp. Mar. Bio. Ecol.*,
578 364(2), 72–79, doi:10.1016/j.jembe.2008.07.003, 2008.

579 Vinther, H. F., Laursen, J. S. and Holmer, M.: Negative effects of blue mussel (*Mytilus edulis*)
580 presence in eelgrass (*Zostera marina*) beds in Flensburg bay, Denmark, *Estuar. Coast. Shelf Sci.*,
581 77(1), 91–103, doi:10.1016/j.ecss.2007.09.007, 2008.

582 Vinther, H. F., Norling, P., Kristensen, P., Dolmer, P. and Holmer, M.: Effects of coexistence
583 between the blue mussel and eelgrass on sediment biogeochemistry and plant performance, *Mar.*
584 *Ecol. Prog. Ser.*, 447, 139–149, doi:10.3354/meps09505, 2012.



- 585 Wahl M., Saderne V., Sawall Y.: How good are we at assessing ocean acidification impact in
586 coastal systems? Limitations, omissions and strengths of commonly used experimental approaches
587 with an emphasis on the neglected role of fluctuations. *Mar. Freshw. Res.*, 2015.
- 588 Wahl, M., S. Schneider Covachã, V. Saderne, C. Hiebenthal, J. D. Müller, C. Pansch, and Y.
589 Sawall. 2017. Macroalgae may mitigate ocean acidification effects on mussel calcification by
590 increasing pH and its fluctuations. *Limnol. Oceanogr.* doi:10.1002/lno.10608
- 591 Waldbusser, G. G., Hales, B., Langdon, C. J., Haley, B. a., Schrader, P., Brunner, E. L., Gray, M.
592 W., Miller, C. a. and Gimenez, I.: Saturation-state sensitivity of marine bivalve larvae to ocean
593 acidification, *Nat. Clim. Chang.*, (December 2014), doi:10.1038/nclimate2479, 2014.
- 594 Yang, B., R. H. Byrne, and M. Lindemuth: Contributions of organic alkalinity to total alkalinity
595 in coastal waters: A spectrophotometric approach. *Mar. Chem.* 176: 199–207.
596 doi:10.1016/j.marchem.2015.09.008, 2015



597 Fig. 1. A. Map of the inner Kiel Bay with study site and the GEOMAR station. B. Photo of the
598 sensor suite at the measurement site.

599 Fig. 2. Deviation between observed and calculated $p\text{CO}_2$ ($\Delta p\text{CO}_2$) as a function of observed $p\text{CO}_2$
600 illustrating the influence of TA_{org} on carbonate system determinations. Dashed lines represent
601 linear regressions of the respective data. **Black triangles:** $\Delta p\text{CO}_2 = p\text{CO}_2 \text{ sensor} - p\text{CO}_2$ (TA, DIC)
602 for the benthic seagrass deployment of this study, $n = 30$. The $\Delta p\text{CO}_2$ can be explained by a
603 combination of the influence of an organic TA contribution of $0.49 \pm 1.47\%$ with measurement
604 uncertainties and sampling errors (spatio-temporal mismatches). **Dark grey diamonds:** $\Delta p\text{CO}_2 =$
605 $p\text{CO}_2 \text{ sensor} - p\text{CO}_2$ (TA, DIC) based on corrected HydroC[®] measurements and discrete samples
606 taken at GEOMAR pier in 2015 (Hiebenthal et al., 2017). DIC, TA and pH_T were measured in the
607 same water samples. The $\Delta p\text{CO}_2$ is due to a TA_{org} fraction of $0.84 \pm 0.0005\%$ (mean \pm SD). **Grey**
608 **circles:** $\Delta p\text{CO}_2 = p\text{CO}_2 \text{ sensor} - p\text{CO}_2$ (DIC, pH_T), based on corrected sensor data and discrete
609 samples taken at GEOMAR pier during the same period in 2015, $n = 18$ (Hiebenthal et al., 2017).
610 There is no $p\text{CO}_2$ dependency of the $\Delta p\text{CO}_2$, because neither DIC nor pH_T are impacted by TA_{org} ,
611 $R^2 = 0.005$. **Solid black line:** Difference between observed and calculated $p\text{CO}_2$ from a model
612 including TA_{org} contributions typical for Baltic Sea water (for details see Appendix B).

613 Fig. 3. Time series for observed parameters: A: Salinity (black) and temperature (grey), 10 min
614 sampling interval B: Total phosphate (green) and silicate (red) concentration from 31 discrete
615 sampling events at the sensor location. C: $p\text{CO}_2$ at 1-min measurement interval (solid line) and
616 24h moving average (dashed line). D: Dissolved oxygen concentration at 10-min measurement
617 interval (solid green line) and as 24h moving average (dashed green line). Also shown is the
618 oxygen saturation concentration calculated from the water temperature and salinity (black). The
619 straight solid red line represents the hypoxia threshold of $60 \mu\text{mol kg}^{-1}$.

620 Fig. 4. Alkalinity (TA) time series (black line) modeled from salinity using the regression
621 equations from August and September. Grey lines represent the TA_{inorg} time series after subtraction
622 of the organic alkalinity contribution of 8 and $30 \mu\text{mol kg}^{-1}$ from TA, respectively. Triangles
623 (August) and dots (September) represent TA of 31 discrete samples used for the regressions. The
624 sample from the 1st of September at 6:40 (open dot) was not considered for the regression. Insert
625 panel: Linear regressions of TA as function of salinity in discrete samples for the months of August



626 in blue (n = 14) and September in red (n= 16), see Table 1 for equations and statistics. Dashed
627 lines are 90% confidence intervals.

628 Fig. 5. Hourly means (\circ) \pm standard deviation (-) for the months of August (grey) and September
629 (black) for Temperature (A.), $p\text{CO}_2$ (B.) and $[\text{O}_2]$ (C.). Hourly mean ranges and maximum upper
630 as well as minimum lower standard deviations (-) calculated using TA_{org} contributions of 8 and 30
631 $\mu\text{mol kg}^{-1}$ for pH_T (D.), DIC (E.), $[\text{CO}_3^{2-}]$ (F.), Ω_{arag} (G.) and Ω_{calc} (H.). The dissolution thresholds
632 of the Ω values are depicted as solid red lines in panel G. and H.

633 Fig. 6. Derived time series of carbonate system parameters: pH_T (A), Dissolved inorganic carbon
634 (DIC, B.) and saturation states for aragonite (Ω_{arag} , light brown) and calcite (Ω_{calc} , dark brown)
635 with dissolution threshold $\Omega = 1$ (red line, C.). All time series are calculated from $p\text{CO}_2$ (10 min
636 interval) and total alkalinity with a mean organic contribution of $19 \mu\text{mol kg}^{-1}$.

637 Fig. 7. Carbonate ion concentration, $[\text{CO}_3^{2-}]$, calculated from $p\text{CO}_2$ (10 min interval) and total
638 alkalinity with a mean organic contribution of $19 \mu\text{mol kg}^{-1}$. The red line represents a side specific
639 $[\text{CO}_3^{2-}]$ threshold of $80 \mu\text{mol kg}^{-1}$ below which calcification declines in mussels according to
640 Thomsen et al., 2015.

641

642

643

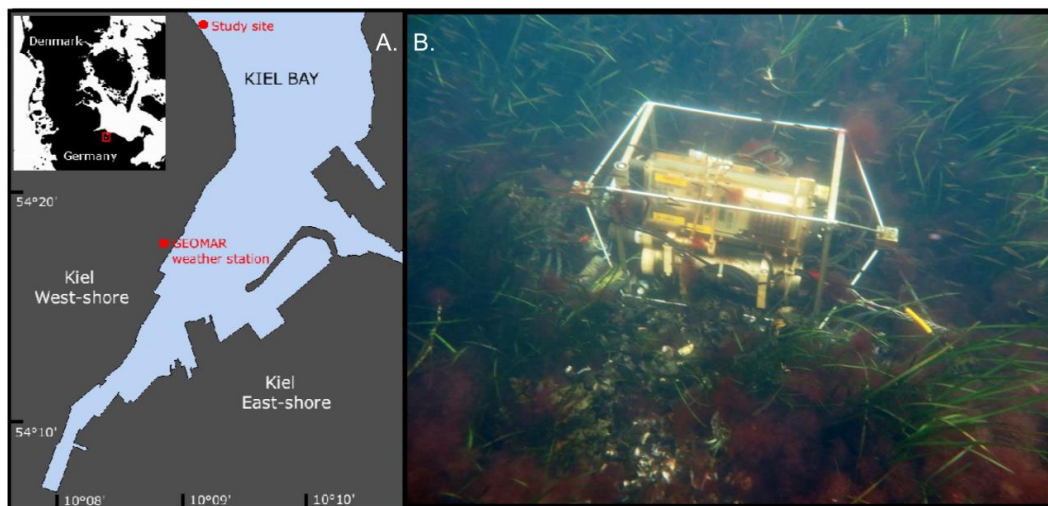
644

645

646

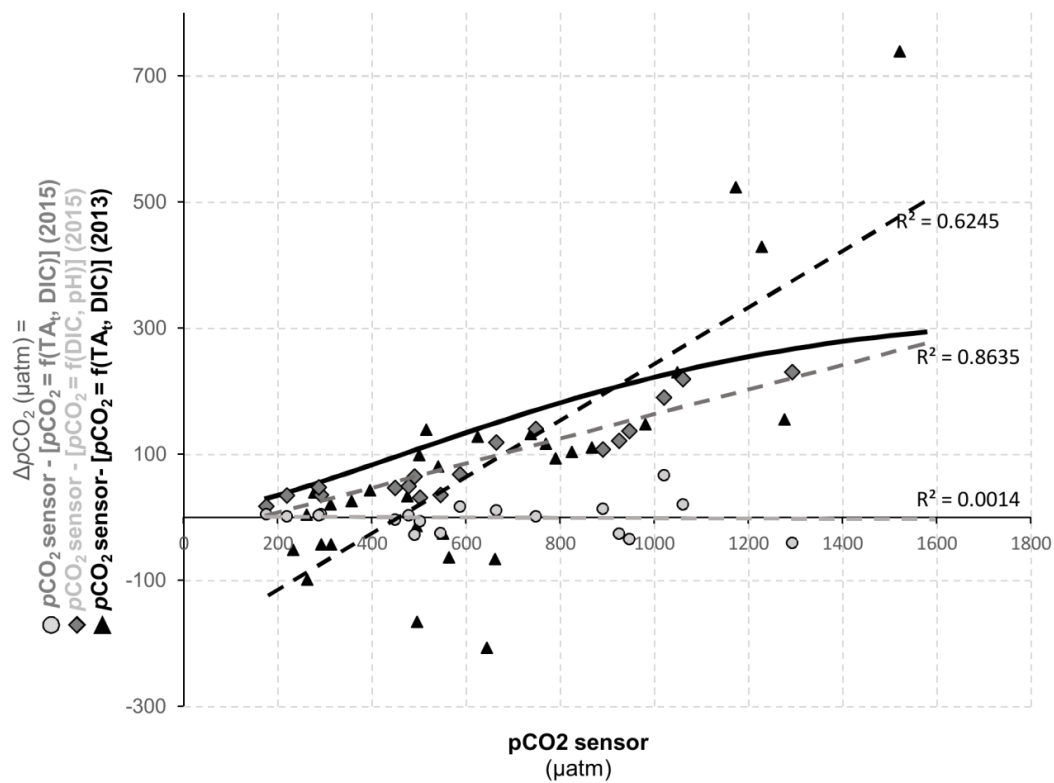
647

648



649

650



651

652

653

654

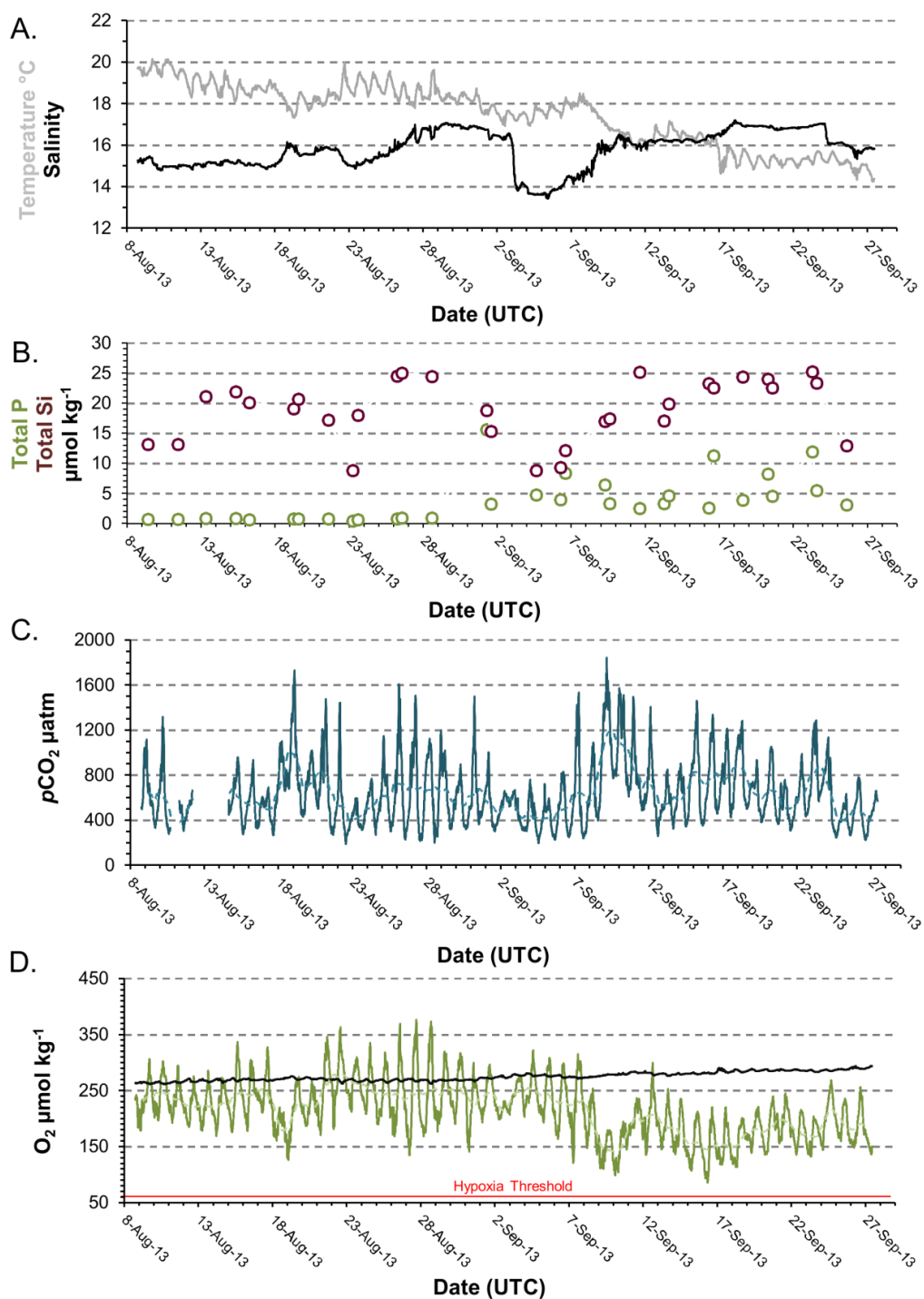
655

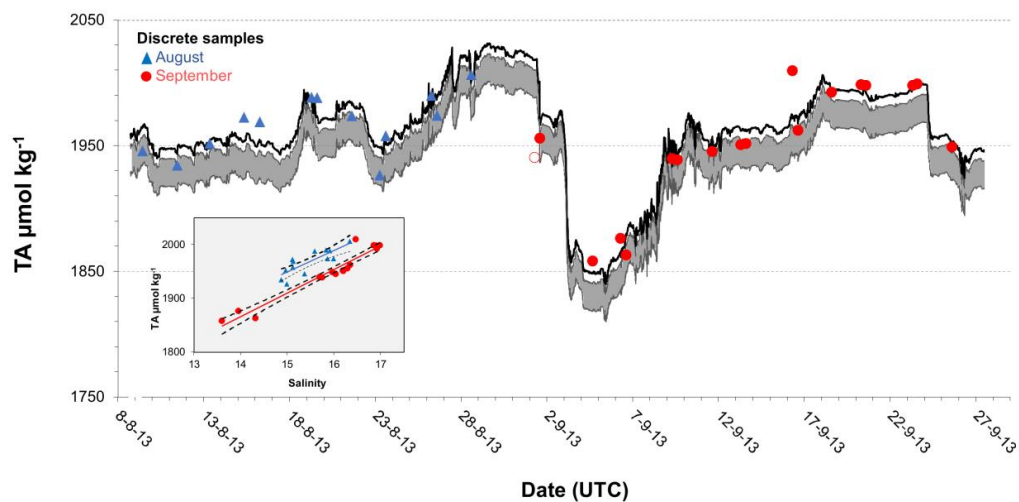
656

657

658

|





660

661

662

663

664

665

666

667

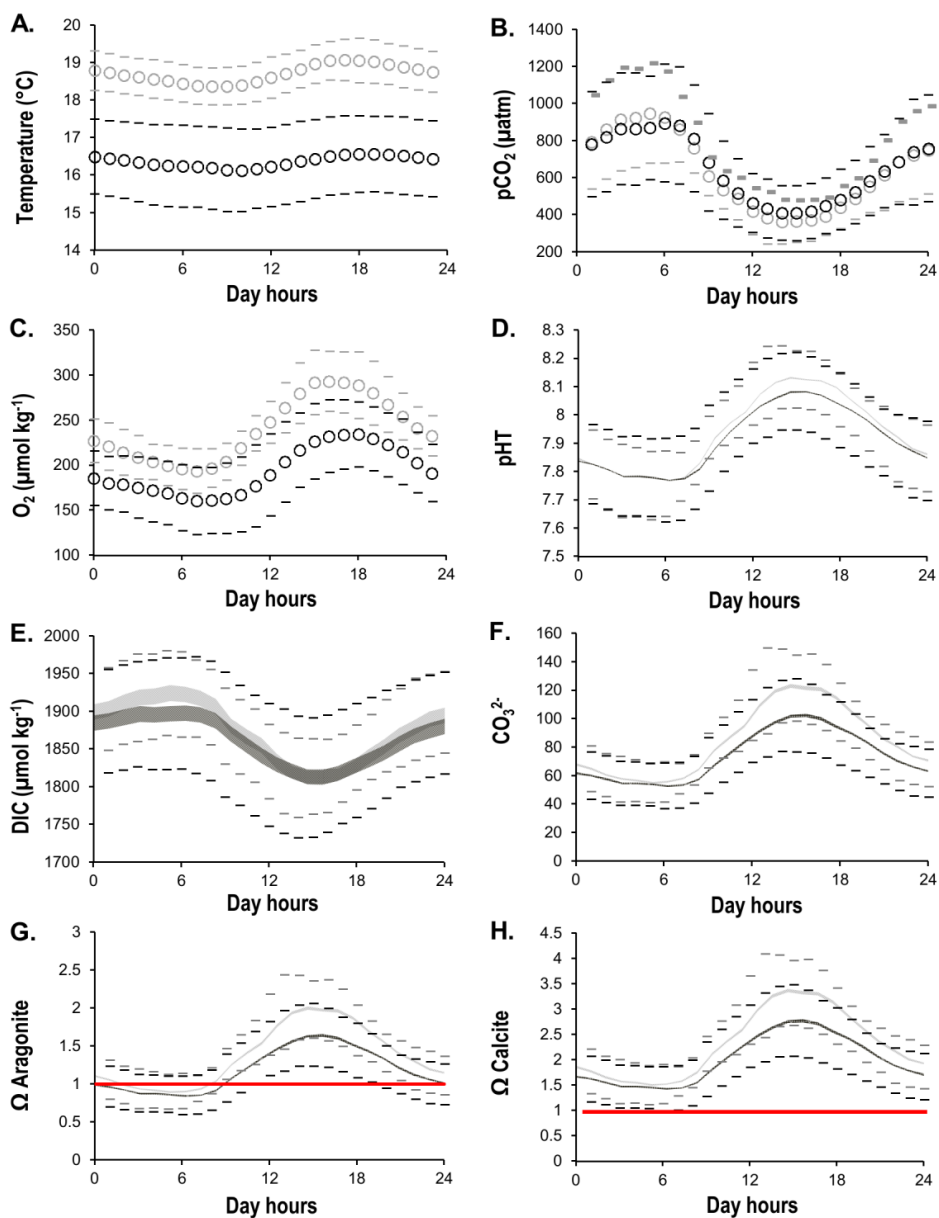
668

669

670

671

|



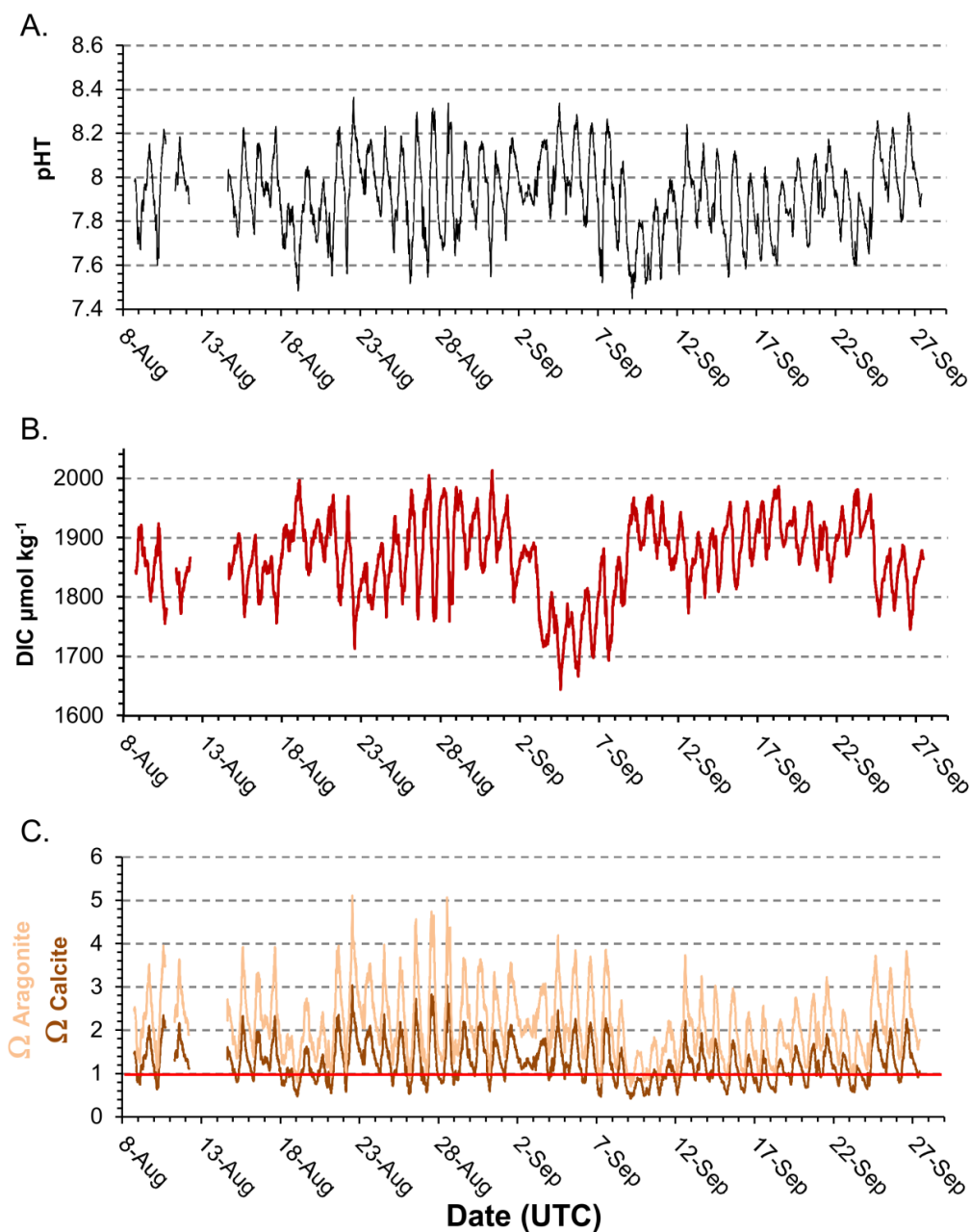
672

673

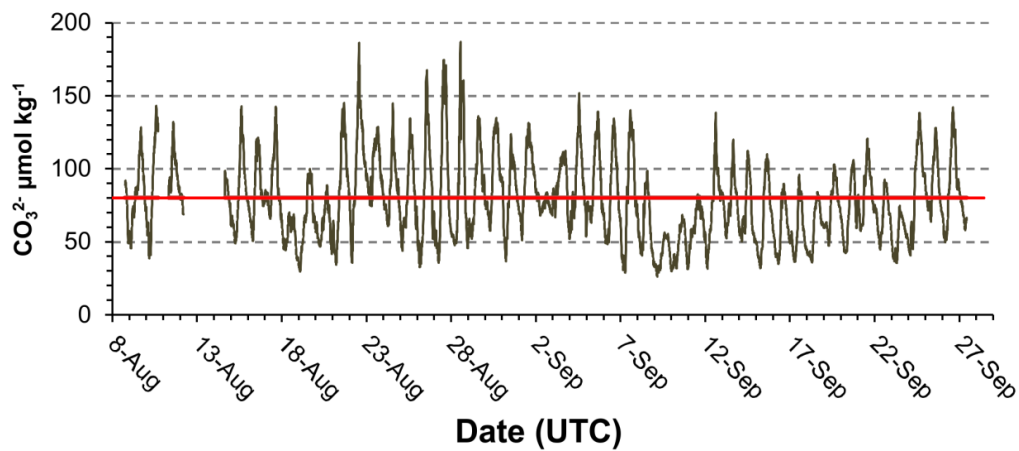
674



675



676



677